HHS Public Access

Author manuscript

Cancer Res. Author manuscript; available in PMC 2019 July 01.

Published in final edited form as:

Cancer Res. 2018 July 01; 78(13): 3560–3573. doi:10.1158/0008-5472.CAN-17-3341.

Alternatively activated macrophages upregulate mesothelial expression of P-selectin to enhance adhesion of ovarian cancer cells

Molly J. Carroll[1], **Kaitlin C. Fogg**[1], **Harin A. Patel**[1], **Harris B. Krause**[1], **Anne-Sophie Mancha**[1,2], **Manish S. Patankar**[3,4], **Paul S. Weisman**[5], **Lisa Barroilhet**[3,4], and **Pamela K. Kreeger**[1,3,4,6]

[1]Department of Biomedical Engineering, University of Wisconsin-Madison, Madison, WI

[2]SURE-REU, University of Wisconsin-Madison, Madison, WI

[3]Department of Obstetrics and Gynecology, University of Wisconsin School of Medicine and Public Health, Madison, WI

[4]University of Wisconsin Carbone Cancer Center, University of Wisconsin School of Medicine and Public Health, Madison, WI

[5]Department of Pathology, University of Wisconsin School of Medicine and Public Health, Madison, WI

[6]Department of Cell and Regenerative Biology, University of Wisconsin School of Medicine and Public Health, Madison, WI

Abstract

Peritoneal metastasis of high-grade serous ovarian cancer (HGSOC) occurs when tumor cells suspended in ascites adhere to mesothelial cells. Despite the strong relationship between metastatic burden and prognosis in HGSOC, there are currently no therapies specifically targeting the metastatic process. We utilized a co-culture model and multivariate analysis to examine how interactions between tumor cells, mesothelial cells, and alternatively-activated macrophages (AAMs) influence the adhesion of tumor cells to mesothelial cells. We found that AAM-secreted MIP-1β activates CCR5/PI3K signaling in mesothelial cells, resulting in expression of P-selectin on the mesothelial cell surface. Tumor cells attached to this *de novo* P-selectin through CD24, resulting in increased tumor cell adhesion in static conditions and rolling under flow. C57/BL6 mice treated with MIP-1β exhibited increased P-selectin expression on mesothelial cells lining peritoneal tissues, which enhanced CaOV3 adhesion *ex vivo* and ID8 adhesion *in vivo*. Analysis of samples from HGSOC patients confirmed increased MIP-1β and P-selectin, suggesting that this novel multi-cellular mechanism could be targeted to slow or stop metastasis in HGSOC by repurposing anti- CCR5 and P-selectin therapies developed for other indications.

Corresponding Author Contact Information: Pamela K. Kreeger, kreeger@wisc.edu, Department of Biomedical Engineering, University of Wisconsin-Madison, 1111 Highland Ave, WIMR 4553, Madison, WI 53705.

Conflict of Interest: The authors declare that they have no competing interests.

Keywords

CCL-4; AAMs; HGSOC; co-culture; metastatic adhesion

Introduction

High grade serous ovarian cancer (HGSOC) is the most lethal gynecological cancer worldwide, with an overall 5-year survival of 46% (1). This dismal prognosis is a result of failure to diagnose most patients prior to the onset of metastasis throughout the peritoneum. Current therapeutics for HGSOC are primarily limited to platinum-based therapies that target proliferating cells (2). However, these therapies are ineffective at inhibiting adhesion and invasion in *in vitro* models of metastasis (3) and no therapies exist to specifically target metastasis. Instead, to combat the spread of HGSOC throughout the peritoneum, a debulking surgery is performed either before chemotherapy or after neoadjuvant treatment. Surgical outcome is a strong predictor of prognosis (4); however, because many tumors have disseminated widely prior to surgery, complete surgical resection is not always possible. Additionally, even with aggressive surgery, microscopic disease remains for most patients, leading to recurrence and complications such as bowel obstructions that can be fatal during a new period of metastasis. Thus, identifying the mechanisms by which HGSOC populates the peritoneum may lead to new therapies and improved outcomes.

HGSOC primarily metastasizes via the transcoelomic route, whereby tumor cells detach from the primary tumor, float through the ascites, and adhere to mesothelial-lined surfaces in the peritoneal cavity (4). During this process, HGSOC cells are likely influenced by numerous elements of the microenvironment, including alternatively activated macrophages (AAMs). In contrast to pro-inflammatory, classically activated macrophages (CAMs), AAMs possess a pro-tumor, anti-inflammatory phenotype and have been linked to remodeling behaviors *in vivo* such as wound healing and tumor progression (5,6). It has been found that AAMs are present in the ascites of many HGSOC patients (7), and experimental evidence supports a role for macrophages in HGSOC metastasis. *In vivo* analysis of ovarian cancer xenograft models treated with clodronate to reduce macrophage levels showed decreased metastasis (8). Clinical studies have found that an increase in tumor AAM-density correlates with advanced disease staging and poor prognosis (9). While *in vitro* co-culture of breast cancer cells with AAMs resulted in increased epithelial-mesenchymal transition (10) and we have previously shown that AAM co-culture with HGSOC cells can induce proliferation (5), the mechanisms by which AAMs in the microenvironment may promote HGSOC metastasis are unknown.

We hypothesized that paracrine signaling from AAMs enhances HGSOC adhesion to mesothelial cells. As the first step to establish a new lesion, changes in this process are expected to impact metastatic burden (11). To address this hypothesis, we modified our co-culture device (12) to create an *in vitro* model of HGSOC encountering the peritoneal lining in the presence of AAMs. Using primary human AAMs in combination with multiple mesothelial and HGSOC lines, we determined the impact of AAMs on HGSOC adhesion to a mesothelial-lined surface. Due to the complex, multi-cellular interactions involved, we

utilized systems biology-based modeling to identify factors secreted by AAMs that enhance adhesion and experimental follow-up to confirm their role and decipher the mechanism by which adhesion increased. Our results suggest that paracrine signaling between AAMs and mesothelial cells alters the proteins expressed on the mesothelial barrier to enhance adhesion of HGSOC and identify novel targets to control the spread of HGSOC.

Materials and Methods

Cell lines and reagents

Unless otherwise stated, all reagents were purchased from ThermoFisher (Waltham, MA). HGSOC cell lines CaOV3, OV-90, and OVCAR3 were purchased from American Type Culture Collection (ATCC; Rockville, MD), OVCAR 4, OVCAR5 and OVCAR8 were obtained from NCI 60 panel (NIH). The LP-9 and LP-3 mesothelial cell lines were purchased from the Coriell Cell Repository (Camden, NJ). All human cell lines were authenticated by human short tandem repeat (STR) analysis at the Experimental Pathology Laboratory at the University of Wisconsin- Madison and mycoplasma testing was conducted using MycoAlert (Lonza; Basel, Switzerland). ID8 cells were obtained from Dr. Katherine Roby (University of Kansas). Cells were maintained at 37°C in a humidified 5% CO2 atmosphere. CaOV3 and OVCAR5 were cultured in a 1:1 (v/v) ratio of MCDB105:Medium199 (Corning; Corning, NY) supplemented with 1% penicillin/streptomycin and 10% heat-inactivated fetal bovine serum (FBS). OV-90, OVCAR3, OVCAR4, and OVCAR8 were cultured in a 1:1 (v/v) ratio of MCDB105: Medium199 supplemented with 1% penicillin/streptomycin and 15% heat-inactivated FBS. LP-9 and LP-3 lines were cultured in a 1:1 (v/v) ratio of Hams F12 (Corning):Medium199 with 1% penicillin/streptomycin, 15% FBS, 2 mM L-glutamine, 10 ng/mL epidermal growth factor, and 0.4 μg/mL hydrocortisone (Corning). ID8 were cultured in DMEM with high glucose, 1% penicillin/streptomycin, 5% heat inactivated FBS, 5 μg/ml insulin, 5 μg/ml transferrin and 5 ng/ml sodium selenite.

Isolation and differentiation of AAMs from whole blood

Whole blood from healthy females over the age of 18 years was purchased from Innovative Research (Novi, MI). Monocytes were enriched by negative selection using the Rosette Sep® monocyte enrichment cocktail according to manufacturer's instructions (STEMCELL Technologies; Vancouver, Canada). To differentiate isolated monocytes into the AAM phenotype, monocytes were seeded on 9 mm square coverslips at a density of 200,000 cells/well for 6 days in AIM V media supplemented with 1% penicillin-streptomycin and 20 ng/mL M-CSF. Macrophages were polarized for 48 hours with 2 ng/mL IL-4 and 2 ng/mL IL-13. AAMs were washed with phosphate buffered saline (PBS) and changed to 1:1 Medium199:MCDB105 supplemented with 1% penicillin/streptomycin (serum free media, SFM) for 24 hours. Control conditions (-AAMs) were prepared by exposing cell-free coverslips to the differentiation protocol to account for the effects of non-specific adsorption of differentiation factors.

In vitro model of adhesion in transcoelomic metastasis

We modified a co-culture device previously developed in our lab (5,12) to construct the *in vitro* model of metastatic adhesion (Supplementary Fig. S1). The device is composed of a PDMS ring that is placed in a well of a 24 well tissue culture plate and a 9×9 mm coverslip placed on top. One or more cell types can be grown within the ring, while another population can be grown on the coverslip. Inverting the coverslip on top of the ring initiates co-culture between the populations. In our model, the tissue culture plastic within the PDMS ring was coated with 1 μg of PureCol Collagen I (Advanced Biomatrix; San Diego, CA) for 2 hours at room temperature. LP-9 or LP-3 were seeded into the PDMS rings to confluency (93,500 cells/cm^2 in 40 μL). Twenty-four hours after seeding, cells were washed with SFM, AAM or control coverslips were placed on top of the PDMS ring, and 40 μL of fresh SFM was added. HGSOC cells were stained with 5 μM CellTracker™ Green CMFDA Dye, dissociated using TrypLE Select Enzyme, and seeded into devices at 10,000 cells/10 μL after 24 hours of mesothelial cell and AAM co-culture. HGSOC cells were allowed to adhere for three hours, then coverslips were removed and devices were washed twice with 2 mL PBS to remove non-adherent cells. Cells within the ring were fixed with 4% paraformaldehyde (Electron Microscopy Sciences; Hatfield, PA) for 15 minutes, washed twice with PBS, and fluorescent HGSOC cells were imaged on a Zeiss Axio Observer.Z1 inverted microscope with an AxioCam 506 mono camera, Plan-NEOFLUOR 20× 0.4-NA air objective, and Zen2 software (Zeiss; Oberkochen, Germany). Five images per well were captured, n=3 wells/condition. Percent adhesion was quantified by converting cells/image to total cells/area of the co-culture device, and dividing by the number of HGSOC cells added to the device.

Confocal imaging of HGSOC adhesion

LP-9 and CaOV3 were stained with 5 μM CellTracker™ Green and 1 μM CellTracker™ Deep Red, respectively. Following completion of the adhesion assay as described above, cultures were imaged with a Nikon AR1S confocal microscope and z-stack reconstructions were created in ImageJ (NIH).

RNA extraction and qRT-PCR

RNA was collected and isolated using the Micro-RNeasy Extraction kit (Qiagen; Valencia, CA), and cDNA was synthesized using the Qiagen FirstStrand Kit according to manufacturer's instructions. cDNA was mixed with Qiagen Mastermix and assayed using the Extracellular Matrix and Adhesion Molecules RT2 Profiler PCR Array (Qiagen) in a CFX real time PCR machine (Bio-Rad; Hercules, CA) for a total of 40 cycles, using Qiagen's Data Analysis Center for analysis. Data is expressed as fold change, with ± 2-fold set as the threshold for significance. qRT-PCR was performed using human primers for *SELP*, *CCR1*, and *CCR5*, and *GAPDH* (all Qiagen), with SsoAdvanced Universal SYBR Green Supermix (Bio-Rad). Three samples were run in duplicate from each condition.

Characterization of MMPs and cytokines

Conditioned media was collected from HGSOC adhesion assays using two unique AAM donors and centrifuged at 1,000g for 15 minutes at 4°C. The supernatant was diluted 1:2 in 1% bovine serum albumin (BSA, Sigma, St. Louis, MO) in SFM and assayed by Bio-Plex

Pro™ Human MMP 9-Plex Panel and Bio-Plex Pro™ Human Cytokine 27-plex Assay (Bio-Rad), using the MagPix® instrument (Luminex Corporation, Austin, TX).

Informed, written consent was obtained from patients recruited under a study approved by the Institutional Review Board at the University of Wisconsin-Madison. Studies were conducted in accordance with recognized ethical guidelines (e.g., Declaration of Helsinki, CIOMS, Belmont Report, U.S. Common Rule). Ascites was collected from patients with HGSOC (n=20) or benign conditions (n=4). Samples were diluted 1:2 in 1% BSA/PBS and assayed using a human MIP-1β DuoSet ELISA following manufacturer's instructions.

PLSR model

The correlation between cytokine and MMP levels and HGSOC adhesion was analyzed by PLSR in SimcaP+ v.12.0.1 (Umetrics; San Jose, CA) with mean-centered and variance-scaled data (13). The independent variable matrix (**X**) consisted of cytokine/MMP levels in culture, and the dependent variable matrix (**Y**) consisted of the percentage of tumor cells that adhered. R^2Y, the coefficient of determination for **Y**, describes how well the model fits the behavior of **Y**. Q^2Y measures the predictive value of the model based upon cross-validation. Components were defined sequentially, and if Q^2Y increased significantly (>0.05) with the addition of the new component, that component was retained, and the algorithm continued until Q^2Y no longer significantly increased.

Interventions in co-culture model

To determine if P-selectin played a role in adhesion, LP-9 in co-culture devices were treated with 10 μg/mL of anti-P-selectin blocking antibody or monoclonal mouse IgG1 isotype (BioLegend; San Diego, CA), or 10 μM of the small molecule P-selectin inhibitor KF38789 or DMSO (0.0005% v/v) 1 hour prior to the addition of ovarian cancer cells. To examine the role of AAM-secreted cytokines on HGSOC adhesion, functional blocking antibodies against IL-13 (1 μg/mL), PDGF-BB (0.5 μg/mL), and MIP-1β (1 μg/mL) or 1 μg/mL polyclonal goat IgG isotype were added to adhesion models during the introduction of the AAM or control coverslip. To determine the impact of MIP-1β on mesothelial expression of *SELP* and HGSOC adhesion, mesothelial cells were treated with MIP-1β for 24 hours. To investigate if MIP-1β regulated *SELP* through CCR5, LP-9 were treated with 100 ng/mL of MIP-1β and 20 μg/mL of CCR5 functional blocking antibody or monoclonal mouse IgG2b isotype (BioLegend) for 24 hours. To test the effectiveness of CCR5 therapeutics, LP-9 were treated with 100 ng/mL of MIP-1β and 10 μg/mL of the CCR5 antagonist maraviroc (Sigma) or DMSO (0.001% v/v) for 24 hours. To inhibit PI3K and MEK pathways, LP-9 were treated with 100 ng/mL of MIP-1β and 10 μM LY294002 or PD0325901 (Sigma), respectively, for 24 hours. To knockdown CD24, HGSOC cells were seeded overnight in a 6 well plate at 10,500 cells/cm^2 in complete growth media without penicillin/streptomycin, treated for 24 hours with 25 nM ON-TARGETplus *CD24* or non-targeting pool siRNA (Dharmacon; Lafayette, CO), washed with PBS, and cultured in complete growth media containing penicillin/streptomycin for 72 hours prior to use in adhesion assay. To determine the impact of MIP-1β in ascites on HGSOC cell adhesion, LP-9 were treated with 10% (v/v) ascites plus 1 μg/mL MIP-1β blocking antibody or 1 μg/mL polyclonal goat IgG isotype for 24 hours prior to addition of HGSOC.

Flow cytometry analysis

LP-9 were seeded at 93,500 cells/cm^2 and treated with 100 ng/mL MIP-1β for 24 hours. Cells were dissociated using trypsin (0.05%)-EDTA (0.02%) and stained with anti-P-selectin (20 ug/mL) or mouse IgG1k isotype (Biolegend) and Alexa Fluor® 488 (1:1000). HGSOC cells were dissociated using TrypLE and stained with CD24-FITC (1 μg/mL), CD162-Alexa Fluor® 647 (0.125 μg/mL), IgG1-FITC isotype, or IgG1-Alexa Fluor® 647 isotype (all BD Biosciences; San Jose, CA) in 2% BSA/PBS and 0.1% sodium azide. CD24 and P-selectin expression was analyzed on a ThermoFisher Attune, and CD162 expression was analyzed on a BD FACSCalibur flow cytometer. Normalized median CD24 expression for each cell was calculated by subtracting the median fluorescent intensity of the isotype control from the median fluorescently intensity of the CD24 stained sample.

HGSOC adhesion to P-selectin

Ibidi 2-well culture inserts (Ibidi; Munich, Germany) were coated with 50 μg/mL P-selectin Fc-chimera or rh IgG1-Fc overnight at room temperature. HGSOC cells were stained with 5 μM CellTracker™ Green, dissociated using TrypLE, and seeded into each chamber of the insert at a concentration of 5,000 cells/40 μL. Cells were allowed to adhere for 3 hours, and percent adhesion was quantified as described above.

HGSOC rolling

LP-9 were seeded to confluency at a concentration of 93,500 cells/cm^2 in a parallel-plate flow chamber (Ibidi μ-Slide VI 0.4, Ibidi). 24 hours later, LP-9 were washed with SFM and treated with 100 ng/mL MIP-1β or 0.1% BSA/PBS for an additional 24 hours, then washed with SFM. CaOV3 cells were stained with 5 μM CellTracker™ Green, dissociated using TrypLE, and suspended in SFM at 100,000 cells/mL. A syringe pump (KD Scientific, Holliston, MA) was used to flow the cancer cells across the LP9 at a shear stress of 0.125 dyn/cm^2 for 30 seconds. Images were captured every 0.5 seconds using time lapse module of the Zen2 software. Instantaneous velocities of the cells were calculated using ImageJ software, and a cell was defined as rolling if it spent greater than five seconds at a mean velocity of less than 50% of the mean velocity of the cells on BSA (14). The rolling flux (cells/mm^2/min) was calculated as the number of rolling cells divided by the area of the field of view and total capture time (14).

AKT and ERK phosphorylation

Following 0, 5, 15, 60, and 240 minutes of treatment with 100 ng/mL MIP-1β, LP-9 were lysed using the Bio-Plex cell lysis buffer (Bio-Rad) according to manufacturer's instructions. Protein concentration was determined through a BCA assay. The levels of AKT (tAKT), pAKT(Thr308), pAKT(S473), ERK, and pERK1/2(Thr202/Tyr204, Thr185/Tyr187) were assayed using the Bio-Plex Pro Magnetic Cell Signaling Assay (Bio-Rad) and read using the MagPix® instrument. The measurement of each phosphorylation site was normalized to the corresponding protein measurement.

In vivo and *ex vivo* mouse studies

Female C57BL/6J (6-12 weeks) were procured from the Research Animal Resource Center Breeding Services (UW-Madison) or Jackson Laboratory (Bar Harbor, ME). All animal protocols were approved by the Institutional Animal Care and Use Committee (IACUC) at the UW-Madison School of Medicine and Public Health. Mice were i.p. injected with 1 μg of recombinant mouse MIP-1β in 100 μL PBS or PBS control. After 24 hours, mice were euthanized by CO_2 asphyxiation, and the peritoneum, omentum, and mesentery were removed for immunohistochemistry or *ex vivo* adhesion assays. Peritoneal wall sections were cut using a biopsy punch, adhered into wells of an 8-well chamber slide, and covered with 400 μL SFM. Cell Tracker Deep Red (1 μM) stained CaOV3 were seeded into chamber slide wells (5,000 cells/100 μL) and allowed to adhere to the peritoneal tissue for 3 hours. Chamber slides were then washed twice with PBS and fixed with 10% formalin for 20 minutes. Fluorescent CaOV3 cells were quantified as cells/cm^2 for the entire tissue.

For *in vivo* adhesion assays, female C57BL/6 mice were i.p. injected with 1 μg recombinant mouse MIP-1β or PBS, and 24 hours later i.p. injected with 300,000 ID8 cells stained with 1 μM Cell Tracker Deep Red. To inhibit P-selectin, mice were treated with KF38789 (1 mg/kg, Tocris; Minneapolis, MN) or DMSO vehicle control (4.8% v/v) 1 hour prior to i.p. injection with ID8 cells. After 90 minutes, mice were euthanized and the peritoneal wall, omentum, and mesentery were removed and whole-mounted onto slides. Fluorescently labeled ID8 cells on the excised tissues were imaged on the Zeiss Axio Observer.Z1. Adhesion was quantified as percent area of tissue covered by adhered ID8.

Immunostaining

LP-9 in co-culture devices were cultured with or without AAMs and treated with 1 μg/mL MIP-1β blocking antibody or polyclonal goat IgG isotype control. LP-9 cells were fixed and immunofluorescence was performed with anti-P-selectin (15 μg/mL) with Alexa Fluor® 488 goat anti-mouse secondary antibody. This antibody is specific for cell-surface P-selectin; additionally, cells were not permeabilized prior to staining. Nuclei were counterstained with Hoechst. P-selectin levels were quantified via mean fluorescence intensity for each image, (n=5 images taken per sample, n=3 samples per condition) using ImageJ. HGSOC were cultured at 10,500 cells/cm^2 overnight under normal growth conditions, fixed, and immunofluorescence was performed with anti-CD24 (BD Biosciences; Franklin Lakes, NJ) or CD15s (1 μg/mL) with Alexa Fluor® 488 goat anti-mouse secondary antibody. LP-9 were cultured at 62,500 cells/cm^2 overnight, and treated with 100 ng/mL MIP-1β for 0, 5, 15, 60, and 240 minutes. Cells were fixed, blocked and permeabilized with 5% goat serum/0.3% Triton X-100/PBS for 1 hour, and immunofluorescence was performed with anti-NF-κβ p65 (Cell Signaling; 1:400) and Alexa Fluor® 488 goat anti-rabbit secondary antibody.

Paraffin-embedded samples of omental tissue from women who underwent omentectomy or omental biopsy for HGSOC staging or non-HGSOC conditions were obtained from archived pathology samples through a protocol approved by the Institutional Review Board at the University of Wisconsin-Madison. Five micron sections were cut and deparaffinization and rehydration was performed prior to heat antigen retrieval using Universal Antigen Retrieval Solution according to manufacturer's instructions. Slides were blocked in tris buffered saline

(TBS, Boston Bioproducts; Ashland, MA) supplemented with 1% BSA and 1% normal goat serum for 1 hour, then incubated overnight at 4°C with antibodies (anti-calretinin (ab702, Abcam; Cambridge, United Kingdom) at 1:50 and anti-P-selectin (15 μg/mL), followed by Alexa Fluor® 488 goat anti-mouse and Alexa Fluor® 594 goat anti-rabbit. Slides were sealed using ProLong® Diamond Antifade Mountant with DAPI.

Paraffin-embedded samples of mouse peritoneal wall, omentum, and mesentery were cut into 5 μm sections and deparaffinization and rehydration were performed as above, prior to heat antigen retrieval using citrate buffer according to manufacturer's instructions. Endogenous peroxidase activity was blocked by incubating slides in 0.3% v/v hydrogen peroxide in methanol for 30 minutes. Slides were blocked overnight at 4°C using diluted horse normal blocking serum in PBS from the VECTASTAIN® ABC-AP Universal Staining Kit (Vector Laboratories; Burlingame, CA). Sections were incubated with mouse anti-CD62p (P-selectin, 5 μg/mL; Biorbyt; Cambridge, United Kingdom) followed by biotinylated universal secondary antibody solution. Sections were then stained with VECTASTAIN ABC Reagent for 30 minutes and ImmPACT DAB Substrate (Vector Laboratories) for 5 minutes. Sections were then stained with Mayer's Hematoxylin Solution for 1 minute and mounted using ClearMount according to manufacturer's instructions. All imaging was performed on the Zeiss Axio Observer Z1 with Axiocam mono camera (fluorescence) or color camera (immunohistochemistry).

Analysis of *CD24* in patient microarray data

The Kaplan-Meier plotter tool (15) was used with the Gene Expression Omnibus and The Cancer Genome Atlas to calculate PFS and OS for stage II-IV and grades II and III patients with *TP53* mutations, split into low and high *CD24* based upon median expression.

Statistical Analysis

All data are presented as mean ± standard deviation. All experiments were performed at least twice, with unique AAM donors used for repeats of co-culture experiments. Statistical calculations (two-sided t-test, two-way ANOVA followed by Bonferroni corrected two-sided t-test, Kolmogorov-Smirnov test, log-rank test) were performed in GraphPad Prism software (La Jolla, California).

Results

AAMs increase HGSOC adhesion to mesothelial cells

To examine the role of AAMs in HGSOC metastasis, we created an *in vitro* model of the peritoneal microenvironment that enables concentrated paracrine signaling (Supplementary Fig. S1A). To simulate the microenvironment of a patient with metastatic disease, and hence an increase in AAM levels, LP-9 mesothelial cells were co-cultured with primary human AAMs for 24 hours. To mimic tumor cells floating in ascites, HGOSC cells in suspension were added to the device on top of the LP-9 and allowed to adhere for three hours (Supplementary Fig. S1B). After removal of non-adherent cells, HGSOC that remained were adhered to the top of the mesothelial monolayer, and had not yet invaded through the LP-9 (Fig. 1A). This is consistent with clinical observations that unlike other cancers, HGSOC

does not infiltrate deeply (16). When AAMs were incorporated in the device, the percentage of HGSOC cells that adhered increased significantly (Fig. 1B and 1C). Consistent with heterogeneity that is observed in HGSOC, baseline adhesion in the absence of AAMs varied among the three lines. However, all three showed increased adhesion with AAMs, suggesting that targeting the mechanism responsible for this increase could impact the extent of tumor metastasis in a broad group of patients. We next examined whether AAM-secreted factors signaled to mesothelial cells (indirect) or tumor cells (direct) to increase HGSOC adhesion (Fig. 1D). To test for indirect signaling, LP-9 were co-cultured with AAMs for 24 hour, and then the AAMs were removed and fresh SFM media was added when HGSOC were seeded into the device. Direct signaling was tested by culturing LP-9 alone for 24 hours, and then adding AAMs and AAM-conditioned media when HGSOC were seeded. Results showed that HGSOC adhesion increased only in the indirect paradigm, suggesting that AAMs induced changes to mesothelial cells to enhance adhesion (Fig. 1E).

AAMs regulate mesothelial expression of P-selectin

Based on our observation that paracrine signals from AAMs enhanced adhesion to LP-9, we hypothesized that AAM-secreted factors upregulated extracellular matrix (ECM) or adhesion proteins on the mesothelial surface that HGSOC could then bind to. To test this hypothesis, we collected mRNA from LP-9 cultured alone or with AAMs and determined that 17 ECM/adhesion-related genes were downregulated, while seven genes were upregulated greater than two-fold (Fig. 1F and Table S1). Of particular interest was the increase in *SELP* (P-selectin), a member of the family of selectin cell adhesion molecules that other tumor cell types have been shown to bind to (17), but has been reported to be absent in mesothelial cells *in vivo* (18) and *in vitro* (19). Validation by qRT-PCR across multiple AAM donors confirmed that LP-9 had a low expression of *SELP*, which was upregulated nearly six-fold during AAM co-culture (Fig. 1G). To test whether P-selectin contributed to HGSOC adhesion, we first examined adhesion of the HGSOC lines to adsorbed P-selectin. All three HGSOC lines had significantly greater adhesion to adsorbed P-selectin compared to Fc control (Fig. 1H). To determine if HGSOC cells were adhering to the mesothelial cells through increased P-selectin, we treated LP-9 with a P-selectin blocking antibody prior to the addition of HGSOC cells. Consistent with the low basal expression of *SELP*, inhibition of P-selectin had no impact on basal adhesion (Fig. 1I). Blocking P-selectin countered the effect of AAM co-culture and returned levels of adhesion to those observed in cultures without macrophages (Fig. 1I). Together, this data suggest that AAMs upregulated *SELP* in mesothelial cells, which results in increased HGSOC adhesion.

Partial least squares regression (PLSR) modeling predicts a role for AAM-secreted MIP-1β in enhanced HGSOC adhesion

We next sought to determine which AAM-secreted molecule(s) were responsible for the increased adhesion of HGSOC. Media was collected from adhesion assays performed with two unique AAM donors and assayed for cytokines, chemokines, and matrix metalloproteinases (MMPs) (Fig. 2A and Table S2). Of the 36 screened ligands, 25 were detectable, with some ligands such as MIP-1β and MMP-7 elevated specifically when AAMs were present. Given the multivariate nature of the data, we utilized PLSR modeling to analyze the correlation between the concentration of secreted ligands and HGSOC

adhesion (13). A two component PLSR model captured the co-variation between ligand secretion and adhesion (R^2Y=0.95) and was highly predictive by cross-validation (Q^2Y= 0.84, Fig. 2B and Supplementary Fig. S2A). Similar to our experimental observations above, conditions separated primarily based on difference across cell lines for the first component of the scores plot, and based on the presence of AAMs in the second component (Supplementary Fig. S2B). Analysis of the loadings (Fig. 2C) and variable importance in projection (VIP, Fig. 2D) identified four ligands (IL-13, MIP-1β/CCL-4, IL-1ra, and PDGF-BB) that clustered closely with adhesion while contributing significantly to the model (VIP>1).

To determine if these ligands were responsible for the increased adhesion, we first examined what was known for each factor in HGSOC. IL-1ra was reported to decrease the extent of metastasis in mouse models of HGSOC (20), but the impact of IL-13, MIP-1β, and PDGF-BB are unknown, suggesting they may mediate the increased adhesion. To examine the impact of these AAM-secreted molecules, mesothelial cells were incubated with neutralizing antibodies against IL-13, PDGF-BB, or MIP-1β during co-culture with AAMs and addition of HGSOC cells. Inhibition of IL-13 and PDGF-BB had no impact on the enhancement of HGSOC adhesion observed with AAMs; however, inhibition of MIP-1β lowered HGSOC adhesion in the presence of AAMs to baseline levels (Fig. 2E and Supplementary Fig. S2C). Analysis of AAM-conditioned media confirmed that AAMs secrete MIP-1β, while HGSOC and mesothelial cells do not (Supplementary Fig. S2D). Levels of MIP-1β were lower in co-culture, suggesting MIP-1β was consumed by the mesothelial and/or HGSOC cells. To determine if MIP-1β was sufficient to increase adhesion in the absence of other AAM-secreted factors, we treated LP-9 with MIP-1β for 24 hours and assayed for adhesion. With MIP-1β treatment, all HGSOC lines had significantly increased adhesion, with levels comparable to the effects seen with AAM co-culture (Fig. 2F). Similar results were observed with an additional mesothelial cell line (LP-3, Supplementary Fig. S2E).

MIP-1β increases mesothelial cell expression of *SELP* through CCR5/PI3K

Given our observations that P-selectin and MIP-1β were each necessary for increased HGSOC adhesion in response to AAMs, we hypothesized that AAM-secreted MIP-1β was responsible for increased *SELP* expression. To test this hypothesis, we inhibited MIP-1β in co-cultures of LP-9 and AAMs with a neutralizing antibody and examined P-selectin levels in LP-9 at both the mRNA and protein level. qRT-PCR results showed that inhibition of MIP-1β significantly decreased *SELP* expression in LP-9 co-cultured with AAMs compared to isotype (Fig. 3A). Immunofluorescent imaging of P-selectin in LP-9 also showed that MIP-1β was necessary for upregulation of P-selectin by AAMs (Figs. 3B and Supplementary Fig. S3A). Treatment of LP-9 with increasing doses of MIP-1β resulted in a dose response of *SELP* expression, confirming that MIP-1β alone was sufficient to induce *SELP* (Fig. 3C). Similarly, treatment of LP-3 mesothelial cells with MIP-1β significantly increased *SELP* expression (Supplementary Fig. S3B). Flow cytometry confirmed that MIP-1β increased mesothelial surface expression of P-selectin on LP-9 (Fig. 3D and Supplementary Fig. S3C). Finally, inhibiting P-selectin mediated adhesion using a selective small molecule inhibitor KF38789 abrogated the increased adhesion in response to MIP-1β

(Fig. 3E), confirming that increased adhesion in response to MIP-1β resulted from increased P-selectin.

As a role for MIP-1β in the regulation of *SELP* expression has not been previously reported, we investigated the intracellular signaling pathways in mesothelial cells responsible for this effect. Both CCR1 and CCR5 are receptors for MIP-1β (21); however, qRT-PCR analysis showed that LP-9 only expressed detectable levels of *CCR5* (Table S3). We treated LP-9 with 100 ng/mL MIP-1β and a CCR5 blocking antibody and determined that blocking CCR5 inhibited MIP-1β–stimulated expression of *SELP* (Fig. 3F). Clinically, CCR5 has been the target of drug development as it is an essential co-receptor for HIV entry. Maraviroc, a CCR5 allosteric modulator approved to treat HIV (22), was also effective in inhibiting MIP-1β–stimulated expression of *SELP* (Fig. 3G). CCR5 has been shown to activate NF-κβ, PI3K and MAPK (23,24), which can regulate *SELP* expression in other cell types (25-27). Immunofluorescent staining of p65 showed no increase in nuclear co-localization upon treatment with MIP-1β (Fig. 3H), suggesting that NF-κβ does not play a role in P-selectin upregulation. Treatment with PD0325901, a MEK inhibitor, significantly decreased *SELP* expression in both vehicle and MIP-1β treated LP-9, suggesting that MEK activation is necessary for even the low basal expression of *SELP* in LP-9 (Fig. 3I). In contrast, inhibition of PI3K with LY294002 had no impact on basal *SELP* expression but significantly reduced the increase in *SELP* observed with MIP-1β treatment (Fig. 3I). Analysis of phosphorylation of ERK and AKT in response to MIP-1β treatment demonstrated no change in pERK, but an increase in pAKT at both Thr308 and Ser473 (Fig. 3J). Combined, these results suggest that MIP-1β activates CCR5 and PI3K to increase *SELP* transcription, and that therapy inhibiting CCR5 activation, such as maraviroc, may be effective in inhibiting *SELP* upregulation.

HGSOC cells adhere to P-selectin through CD24

We next sought to determine which ligands are expressed on HGSOC cells to enable binding to P-selectin. The primary ligand for P-selectin, CD162 (PSGL-1), is expressed in neutrophils and lymphocytes (28), but has not been evaluated in HGSOC lines. Flow cytometry analysis indicated that none of the HGSOC lines in our panel expressed detectable levels of CD162 (Fig. 4A top panel). Alternatively, CD24 has been reported to act as a ligand for P-selectin (17) and its overexpression is correlated with a poor prognosis in HGSOC patients (29). When we examined our lines, all expressed detectable levels of CD24, with the greatest surface expression in CaOV3 and the weakest in OVCAR5 (Fig. 4A bottom panel and Supplementary Fig. S4A,B). It has been shown that expression of siayl-Lewis(x) (CD15s) is necessary for CD24 to bind to P-selectin (17). When examined by immunofluorescent imaging, CaOV3 had the highest expression of CD15s and OVCAR5 had the lowest expression, similar to the pattern observed with CD24 (Fig. 4B). Given the variation in CD24/CD15s levels and the magnitude of increase in adhesion levels with AAM co-culture (Fig. 1C), we examined the relationship between CD24 expression and the fold-change in percentage of cells that adhere with AAMs present. We expanded our panel of HGSOC cells to 6 lines and identified a correlation between CD24 expression and the fold change in HGSOC adhesion to LP-9 treated with MIP-1β (Fig. 4C and Supplementary Fig. S5A,B), suggesting that CD24 may be responsible for this effect. To examine this finding in more detail, we treated HGSOC cell lines with non-targeted (si*C*) or CD24-targeted

(si*CD24*) siRNA and assayed adherence to LP-9 treated with MIP-1β or vehicle. While CD24 knockdown had no impact on baseline adhesion, the loss of CD24 significantly reduced adhesion in the presence of AAMs for all HGSOC cell lines (Fig. 4D and Supplementary Fig. S5C,D), suggesting a role for CD24 adhesion to P-selectin in the presence of AAMs and providing a potential explanation for the correlation between CD24 levels and prognosis (29).

Upregulation of P-selectin on LP-9 induces rolling of HGSOC cells under flow

While our analysis of the interactions between AAMs, mesothelial cells, and HGSOC presented in Figs. 1-4 were conducted in static conditions, the peritoneal cavity is a complex environment subject to slow fluid flow as well as stagnant pockets (30). Selectins are best known for inducing rolling that slows leukocytes and supports integrin engagement (31). In particular, P-selectin has been shown to aid in the rolling of breast cancer cells along endothelial cells (17). To determine if this same rolling phenomenon occurred between HGSOC and mesothelial cells, we evaluated the ability of MIP-1β-treated LP-9 to induce rolling of HGSOC cells in a parallel plate flow chamber. CaOV3 exhibited slower velocities (Fig. 4E) and significantly more cell rolling on MIP-1β-treated LP-9 surfaces (Fig. 4F). The results of these dynamic flow experiments suggest that MIP-1β-upregulation of P-selectin in mesothelial cells increases rolling of HGSOC cells, which would translate to increased metastatic potential in regions of the peritoneal cavity that are subject to fluid flow.

MIP-1β increases P-selectin expression and adhesion of HGSOC *in vivo*

We next sought to validate the proposed MIP-1β/P-selectin mechanism *in vivo*. C57BL/6 mice were injected with vehicle control or 1 μg MIP-1β intraperitoneally (i.p.). Similar to the human mesothelial lines, P-selectin on the mesothelial cells of peritoneal wall, omentum, and mesentery was increased in response to MIP-1β (Fig. 5A and Supplementary Fig. S6A-C). Next, we sought to determine whether this increase in P-selectin increased the adhesion of CD24+ HGSOC cells to peritoneal tissues. Adhesion of CaOV3 cells to excised peritoneal wall tissue was assayed *ex vivo*, and found to be significantly increased with MIP-1β treatment (Fig. 5B). Additionally, we utilized the syngeneic HGSOC model (ID8 cells and C57BL/6 mice) (32) in combination with vehicle/MIP-1β (Fig. 5C,D). As with our *in vitro* and *ex vivo* results, ID8 adhesion to the peritoneal wall, mesentery, and omentum was significantly increased with MIP-1β. To test the link between increased P-selectin and increased adhesion, mice were treated with KF38789 or DMSO control prior to injection of ID8 cells. As with our *in vitro* studies using human cells, the MIP-1β induced increase in adhesion was lost when P-selectin was inhibited.

MIP-1β, CD24, and P-selectin are upregulated during HGSOC progression

Previous analyses has shown that MIP-1β is elevated in the ascites of ovarian, fallopian tube, and peritoneal cancer patients compared to serum levels (33); however, to our knowledge, no studies have compared MIP-1β levels between ascites from HGSOC patients and those with benign conditions. Therefore, we collected ascites from patients undergoing surgery for benign conditions or HGSOC debulking, and determined that MIP-1β was significantly elevated in HGSOC (Fig. 6A). Ascites is a complex mixture of multiple components, some of which could potentially influence the effects of MIP-1β on mesothelial cells. Therefore,

we treated LP-9 with HGSOC ascites from the three patients with the highest levels of MIP-1β. Our results demonstrated that HGSOC adhesion increased significantly in response to ascites and that MIP-1β inhibition was sufficient to offset this effect (Fig. 6B and Supplementary Fig. S7).

Using the Kaplan Meier plotting tool and data from over 400 primary HGSOC tumors in the Gene Expression Omnibus and The Cancer Genome Atlas (15), we found that higher expression of *CD24* was correlated with shorter progression free survival (PFS) in HGSOC patients (Fig. 6C and Table S4). This suggests that patients with tumor cells expressing CD24 have faster recurring disease, possibly through enhanced metastatic spread due to P-selectin/CD24 interactions. Finally, we collected omental tissue from non-HGSOC and HGSOC patients and stained for P-selectin and calretinin (a mesothelial marker (34)). In omental samples that did not involve HGSOC, P-selectin was not detected in mesothelial cells (Fig. 6D and Supplementary Fig. S8A-C), consistent with prior reports (18). In contrast, P-selectin was expressed in the omentum from HGSOC patients, and co-localized with the calretinin marker (Fig. 6D and Supplementary Fig. S8C). Quantification confirmed that mesothelial cells from HGSOC patients had significantly elevated P-selectin (Fig. 6E), suggesting that inhibiting P-selectin/CD24 interactions may be an effective method to slow or stop metastasis in HGSOC.

Discussion

Through the use of an *in vitro* model mimicking the HGSOC metastatic microenvironment and multivariate analysis, we determined that AAM-secreted MIP-1β increased adherence of HGSOC to mesothelial cells. Further, through multiple experimental approaches, we decoded the mechanism by which MIP-1β's actions were achieved. Our results demonstrate that through AAM-secreted MIP-1β, CCR5 is activated on mesothelial cells, upregulating P-selectin, and leading to increased adhesion of HGSOC cells through P-selectin/CD24 interactions. Furthermore, this mechanism was validated using *in vivo* models and HGSOC patient data. These results indicate a mechanism by which AAMs educate the microenvironment to enhance HGSOC progression, and identified multiple targets for which therapies to slow or stop HSGOC metastasis can be developed and tested.

Previous studies have demonstrated that elements of the microenvironment influence HGSOC metastasis. For example, Kenny et al. identified that incorporation of fibroblasts in a biomimetic model of the human omentum enhanced ovarian cancer adhesion to mesothelial cells (35); however, they were unable to identify the precise mechanism involved, suggesting that culture models with greater flexibility would be beneficial. In contrast to co-culture models where the cells can have physical contact, our co-culture maintains cells on separate surfaces that can be brought together or separated as needed to examine the dynamics of paracrine cellular interactions. Through this feature, we were able to determine that the effects of AAM secreted factors on mesothelial cells were essential for enhanced tumor cell adhesion. Identifying the specific secreted factor or factors responsible for this enhanced adhesion was non-trivial, as our co-cultures were positive for 27 of the 36 ligands assayed. To begin narrowing our search, we hypothesized that levels of factors present in our cultures would correlate with the percentage of adherent HGSOC and utilized

PLSR, a multivariate modeling approach that emphasizes co-variation between an independent and dependent data set. While PLSR has been most widely used in the systems biology field to examine the relationship between signaling events and downstream cellular phenotypes (36), it has also been used to examine how protein levels correlate to outcomes such as drug treatment in HGSOC (37). Our use of this modeling technique suggested a strong correlation for only four secreted factors, simpifying our attempts to unravel the mechanism of action.

Of course, correlation does not equal causation, so we sought to validate the potential role of the suggested ligands through a combination of neutralization experiments and treatment with the candidate factor in the absence of other AAM secreted factors. These results indicated that MIP-1β was necessary and sufficient for the observed increase in tumor adhesion, but an analysis of the current literature did not indicate a clear role for MIP-1β in HGSOC. For example, the concentration of MIP-1β in serum was reported to be lower in HGSOC patients compared to benign patients (38). However, matched ascites and serum samples from HGSOC patients indicated that the concentration of MIP-1β was higher in ascites compared to serum levels (33) suggesting that MIP-1β is concentrated in the peritoneal microenvironment of HGSOC patients. Therefore, we sought to compare the levels of peritoneal MIP-1β between benign conditions and HGSOC patients, and determined the MIP-1β was significantly elevated in HGSOC. This study is to our knowledge the first to compare these conditions, likely due to the limited availability of peritoneal fluid from women with benign conditions. MIP-1β has been detected in HGSOC biopsies (39) but we did not observe detectable levels in media from HGSOC or mesothelial cells, suggesting that other cells in the microenvironment may be the source of MIP-1β. A prior investigation found that the presence of CD68+ macrophages in the stroma did not correlate to MIP-1β levels (40); however, this study did not further characterize the macrophages into the classically-activated macrophage (CAM) or AAM phenotype and the ratio of AAMs:CAMs varies between HGSOC patients (9). In our analysis of factors secreted in our *in vitro* model, we showed that AAMs secreted MIP-1β. It has previously been shown that treatment of primary macrophages with ovarian cancer cell supernatant resulted in a strong AAM phenotype, and upregulation greater than 500-fold of MIP-1β (41). Therefore, is it possible that rather than total macrophage levels, the density of AAMs may correlate to MIP-1β in HGSOC biopsies. Intriguingly, fibroblasts secrete MIP-1β upon stimulation with TNFα (42), which is produced by tumor-associated AAMs (43). These cell signaling interactions suggest that AAMs not only secrete MIP-1β, but may stimulate its secretion in other secondary cells of the HGSOC microenvironment, further driving metastatic adhesion.

We next sought to understand what elements of the mesothelial cells were altered by MIP-1β to increase adhesion. Through a qRT-PCR screen, we identified changes in *SELP* expression and validated that P-selectin was responsible for HSGOC cell adhesion. Immunostaining of omental biopsies from HGSOC patients and peritoneal organs from MIP-1β-treated mice demonstrated increased P-selectin expression. Furthermore, *in vivo* treatment with MIP-1β increased the adhesion of CaOV3 and ID8 cells *ex vivo* and *in vivo* respectively. Additionally, we determined that CCR5/PI3K signaling was responsible for the upregulation of P-selectin by MIP-1β. This link that has not been documented in any cell type, but is

supported by evidence that endothelial cell expression of P-selectin is controlled by PI3K/AKT pathway (25). In regards to HGSOC, stimulation of peritoneal mesothelial cells with ascites activated the PI3K pathway (44), although the specific factor or factors responsible for this effect was not determined. In a Phase II study (NCT01283035) of the AKT inhibitor MK2206 in platinum-resistant ovarian cancer patients with a mutations in PI3K or AKT, 80% of the patients developed stable disease (45). While this clinical trial was designed to target the PI3K/AKT pathway in tumor cells, our findings suggest there may be potential benefit within the tumor microenvironment stroma when targeting this pathway.

While our experimental results clearly demonstrated an important role for P-selectin in the increased adhesion of tumor cells to mesothelial cells, the extent of adhesion of tumor cells to adsorbed P-selectin was lower than we expected. However, our initial experiments were done under static conditions and P-selectin is best known for inducing rolling under flow through the use of both slip- and catch-bonds (46). As HGSOC metastasizes by the transcoelomic route, tumor cells will be subject to the flow conditions that are inherent to the peritoneal cavity (30). When we examined HGSOC adhesion to mesothelial cells under flow, we saw no evidence of rolling in the absence of MIP-1β, when mesothelial cells are P-selectin negative. In contrast, an increased number of tumor cells rolled and had lower velocities on MIP-1β treated mesothelials that express P-selectin. Therefore, upregulation of P-selectin may be crucial to bring tumor cells under physiological flow conditions into close proximity with mesothelial cells for integrin engagement, such as occurs with leukocyte rolling (31). Indeed, we found that MIP-1β enhanced ID8 *in vivo* adhesion in a P-selectin dependent manner. Varying integrin expression may be responsible for the observed heterogeneity in baseline adhesion of HGSOC to mesothelial cells in static conditions.

To complete our understanding of this multi-cellular mechanism, we sought to identify the tumor cell ligand responsible for the adhesion to mesothelial cells. While PSGL-1 has been shown to be expressed in neutrophils and binds to P-selectin on endothelial cells (28), our data demonstrated that our panel of HGSOC lines do not express PSGL-1. However, all HGSOC lines we tested expressed CD24, which has been shown to initiate breast cancer rolling along P-selectin on endothelial cells (17). Interestingly, clinical studies have identified CD24 as a biomarker of poor prognosis and indicative of an invasive phenotype in ovarian cancer (29). Additionally, our analysis of TCGA data found that high expression of *CD24* correlated with worse PFS. Despite these correlations, the mechanisms by which CD24 influence HGSOC metastasis are not well understood, and much of the effect of CD24 has been attributed to its identification as a marker of cancer stem cells (47). Using quantitative approaches, we showed that CD24 levels correlated to the fold-change in adhesion that the MIP-1β/P-selectin mechanism induced, and further that knockdown of CD24 inhibited AAM-enhanced adhesion to mesothelial cells. Thus, our study illustrates a novel mechanism by which CD24 enhances the metastasis of HGSOC via its interaction with P-selectin on mesothelial cells in the tumor microenvironment.

Excitingly, there are already clinical agents in development for other diseases that could be repurposed to target elements of this pathway in transcoelomic metastasis. As noted above, trials for AKT inhibitors have been conducted for patients with mutations in PI3K or AKT2 (45), but could potentially be broadened to examine the impact of inhibiting AKT activation

in the microenvironment. For a more specific therapy, two monoclonal antibodies against P-selectin, crizanlizumab (48) and inclacumab (49), have been developed to treat sickle cell anemia and myocardial damage following a heart attack, respectively. Both antibodies were well tolerated in patients when administered systemically. Our analysis of patient samples confirmed the P-selectin is dysregulated (*i.e.*, present) in patients with HGSOC. Our *in vitro* and *in vivo* tests with an anti-P-selectin antibody and small molecular inhibitor demonstrated that this approach was able to inhibit tumor cell adhesion. Excitingly, crizanlizumab may have additional potency as it has been shown to not only block ligand binding but also disrupt existing P-selectin-ligand interactions (50). Alternatively, drugs targeting CCR5, such as the allosteric inhibitor maraviroc, have been developed due to the role of CCR5 as a co-receptor for HIV (22). Our analysis of patient samples demonstrated that MIP-1β is elevated in HGSOC and maraviroc inhibited the upregulation of *SELP* in mesothelial cells in our *in vitro* model.

In additional to the clear translational potential of our findings for HGSOC, our work has broader implications for the cancer field. First, our results emphasize the complex role of the tumor microenvironment. While prior results, including our own (5), have demonstrated that cells in the tumor microenvironment can direct tumor cell behaviors, our results here show that the impact of microenvironment cells on each other must also be examined. Broadening our analysis of the tumor microenvironment to include these higher order interactions may reveal new treatment strategies.

Supplementary Material

Refer to Web version on PubMed Central for supplementary material.

Acknowledgments

We thank the University of Wisconsin Carbone Cancer Center Experimental Pathology Laboratory, Flow Cytometry Laboratory, and Microtechnology Core supported by NIH 5P30CA014520, the University of Wisconsin Optimal Imaging Core Facility, and the RARC Breeding services. We thank Dr. Shigiki Miyamoto for the NFκβ reagents, and the members of the Kreeger laboratory for helpful discussions with this manuscript. Finally, we are indebted to our late colleague Dr. Patricia Keely for insights she provided as this story progressed. Funding was provided by the American Cancer Society (RSG-13-026-01-CSM and Midwest Division supplement, P. Kreeger), NIH (1DP2CA195766, P. Kreeger; 1R21CA143616, M. Patankar; R25GM083252, H. Krause, CCITLA supplement to 5P30CA014520, L. Barroilhet), Marsha Rivkin Center for Ovarian Cancer Research Pilot Grant (P. Kreeger), Marsha Rivkin Center for Ovarian Cancer Research Scientific Scholar Fellowship (K. Fogg), NSF Graduate Research Fellowship (M. Carroll), Wisconsin Alumni Research Foundation (M. Carroll), Department of Defense (W81XWH-04-1-0102, M. Patankar), Department of Obstetrics and Gynecology intramural funding (M. Patankar), charitable donation from Jean McKenzie (M. Patankar), and Wisconsin Ovarian Cancer Alliance (M. Patankar).

References

1. Siegel RL, Miller KD, Jemal A. Cancer statistics, 2016. CA Cancer J Clin. 2016; 66:7–30. [PubMed: 26742998]
2. Luvero D, Milani A, Ledermann JA. Treatment options in recurrent ovarian cancer: latest evidence and clinical potential. Therapeutic advances in medical oncology. 2014; 6:229–39. [PubMed: 25342990]
3. Kenny, Ha, Lal-Nag, M., White, Ea, Shen, M., Chiang, C-Y., Mitra, AK., et al. Quantitative high throughput screening using a primary human three-dimensional organotypic culture predicts in vivo efficacy. Nature communications. 2015; 6:6220.

4. Lengyel E. Ovarian cancer development and metastasis. The American journal of pathology. 2010; 177:1053–64. [PubMed: 20651229]
5. Carroll MJ, Kapur A, Felder M, Patankar MS, Kreeger PK. M2 macrophages induce ovarian cancer cell proliferation via a heparin binding epidermal growth factor/matrix metalloproteinase 9 intercellular feedback loop. Oncotarget. 2016
6. Novak ML, Koh TJ. Macrophage phenotypes during tissue repair. J Leukoc Biol. 2013; 93:875–81. [PubMed: 23505314]
7. Reinartz S, Schumann T, Finkernagel F, Wortmann A, Jansen JM, Meissner W, et al. Mixed-polarization phenotype of ascites-associated macrophages in human ovarian carcinoma: Correlation of CD163 expression, cytokine levels and early relapse. International Journal of Cancer. 2014; 134:32–42. [PubMed: 23784932]
8. Reusser NM, Dalton HJ, Pradeep S, Gonzalez-Villasana V, Jennings NB, Vasquez HG, et al. Clodronate inhibits tumor angiogenesis in mouse models of ovarian cancer. Cancer Biol Ther. 2014; 15:1061–7. [PubMed: 24841852]
9. Zhang M, He Y, Sun X, Li Q, Wang W, Zhao A, et al. A high M1/M2 ratio of tumor-associated macrophages is associated with extended survival in ovarian cancer patients. Journal of Ovarian Research. 2014; 7:19. [PubMed: 24507759]
10. Su S, Liu Q, Chen J, Chen J, Chen F, He C, et al. A Positive Feedback Loop between Mesenchymal-like Cancer Cells and Macrophages Is Essential to Breast Cancer Metastasis. Cancer Cell. 2014; 25:605–20. [PubMed: 24823638]
11. Worzfeld T, Pogge von Strandmann E, Huber M, Adhikary T, Wagner U, Reinartz S, et al. The Unique Molecular and Cellular Microenvironment of Ovarian Cancer. Front Oncol. 2017; 7:24. [PubMed: 28275576]
12. Carroll MJ, Stopfer LE, Kreeger PK. A simplified culture system to examine soluble factor interactions between mammalian cells. Chemical communications (Cambridge, England). 2014; 50:5279–81.
13. Kreeger PK. Using partial least squares regression to analyze cellular response data. Science Signaling. 2013; 6:tr7. [PubMed: 23592846]
14. Lee D, King MR. Microcontact printing of P-selectin increases the rate of neutrophil recruitment under shear flow. Biotechnol Prog. 2008; 24:1052–9. [PubMed: 19194913]
15. Gyorffy B, Lánczky A, Szállási Z. Implementing an online tool for genomewide validation of survival-associated biomarkers in ovarian-cancer using microarray data from 1287 patients. Endocrine-Related Cancer. 2012; 19:197–208. [PubMed: 22277193]
16. Bristow RE, del Carmen MG, Kaufman HS, Montz FJ. Radical oophorectomy with primary stapled colorectal anastomosis for resection of locally advanced epithelial ovarian cancer. J Am Coll Surg. 2003; 197:565–74. [PubMed: 14522325]
17. Aigner S, Ramos CL, Hafezi-Moghadam A, Lawrence MB, Friederichs J, Altevogt P, et al. CD24 mediates rolling of breast carcinoma cells on P-selectin. FASEB journal: official publication of the Federation of American Societies for Experimental Biology. 1998; 12:1241–51. [PubMed: 9737727]
18. Chung-Welch N, Patton WF, Shepro D, Cambria RP. Human omental microvascular endothelial and mesothelial cells: characterization of two distinct mesodermally derived epithelial cells. Microvasc Res. 1997; 54:108–20. [PubMed: 9327382]
19. Gebauer F, Wicklein D, Stübke K, Nehmann N, Schmidt A, Salamon J, et al. Selectin binding is essential for peritoneal carcinomatosis in a xenograft model of human pancreatic adenocarcinoma in pfp–/rag2– mice. Gut. 2013; 62:741–50. [PubMed: 22490524]
20. Lewis AM, Varghese S, Xu H, Alexander HR. Interleukin-1 and cancer progression: the emerging role of interleukin-1 receptor antagonist as a novel therapeutic agent in cancer treatment. Journal of Translational Medicine. 2006; 4:48. [PubMed: 17096856]
21. Seki E, De Minicis S, Gwak GY, Kluwe J, Inokuchi S, Bursill CA, et al. CCR1 and CCR5 promote hepatic fibrosis in mice. Journal of Clinical Investigation. 2009; 119:1858–70. [PubMed: 19603542]
22. Maeda K, Das D, Nakata H, Mitsuya H. CCR5 inhibitors: emergence, success, and challenges. Expert Opin Emerg Drugs. 2012; 17:135–45. [PubMed: 22533737]

23. Allen SJ, Crown SE, Handel TM. Chemokine: Receptor structure, interactions and antagonism. Annual Review of Immunology. 2007; 25:787–820.
24. Fantuzzi L, Spadaro F, Purificato C, Cecchetti S, Podo F, Belardelli F, et al. Phosphatidylcholine-specific phospholipase C activation is required for CCR5-dependent, NF-kB-driven CCL2 secretion elicited in response to HIV-1 gp120 in human primary macrophages. Blood. 2008; 111:3355–63. [PubMed: 18203956]
25. Ghoshal P, Rajendran M, Odo N, Ikuta T. Glycosylation inhibitors efficiently inhibit P-selectin-mediated cell adhesion to endothelial cells. PLoS ONE. 2014; 9
26. Qiu W, Chen N, Zhang Q, Zhuo L, Wang X, Wang D, et al. Resistin increases platelet P-selectin levels via p38 MAPK signal pathway. Diab Vasc Dis Res. 2014; 11:121–4. [PubMed: 24396117]
27. Wang Y, Wang X, Sun M, Zhang Z, Cao H, Chen X. NF-kB activity-dependent P-selectin involved in ox-LDL-induced foam cell formation in U937 cell. Biochem Biophys Res Commun. 2011; 411:543–8. [PubMed: 21763287]
28. Xu T, Zhang L, Geng ZH, Wang HB, Wang JT, Chen M, et al. P-selectin cross-links PSGL-1 and enhances neutrophil adhesion to fibrinogen and ICAM-1 in a Src kinase-dependent, but GPCR-independent mechanism. Cell Adh Migr. 2007; 1:115–23. [PubMed: 19262138]
29. Kristiansen G, Denkert C, Schlüns K, Dahl E, Pilarsky C, Hauptmann S. CD24 is expressed in ovarian cancer and is a new independent prognostic marker of patient survival. The American journal of pathology. 2002; 161:1215–21. [PubMed: 12368195]
30. Meyers MA. Distribution of intra-abdominal malignant seeding: dependency on dynamics of flow of ascitic fluid. Am J Roentgenol Radium Ther Nucl Med. 1973; 119:198–206.
31. McEver RP. Selectins: initiators of leucocyte adhesion and signalling at the vascular wall. Cardiovasc Res. 2015; 107:331–9. [PubMed: 25994174]
32. Roby KF, Taylor CC, Sweetwood JP, Cheng Y, Pace JL, Tawfik O, et al. Development of a syngeneic mouse model for events related to ovarian cancer. Carcinogenesis. 2000; 21:585–91. [PubMed: 10753190]
33. Giuntoli RL, Webb TJ, Zoso A, Rogers O, Diaz-Montes TP, Bristow RE, et al. Ovarian cancer-associated ascites demonstrates altered immune environment: Implications for antitumor immunity. Anticancer Research. 2009; 29:2875–84. [PubMed: 19661290]
34. Barberis MC, Faleri M, Veronese S, Casadio C, Viale G. Calretinin. A selective marker of normal and neoplastic mesothelial cells in serous effusions. Acta cytologica. 1997; 41:1757–61. [PubMed: 9390137]
35. Kenny HA, Krausz T, Yamada SD, Lengyel E. Use of a novel 3D culture model to elucidate the role of mesothelial cells, fibroblasts and extra-cellular matrices on adhesion and invasion of ovarian cancer cells to the omentum. International Journal of Cancer. 2007; 121:1463–72. [PubMed: 17546601]
36. Janes KA, Albeck JG, Gaudet S, Sorger PK, Lauffenburger DA, Yaffe MB. A systems model of signaling identifies a molecular basis set for cytokine-induced apoptosis. Science (New York, NY). 2005; 310:1646–53.
37. Prasasya RD, Vang KZ, Kreeger PK. A multivariate model of ErbB network composition predicts ovarian cancer cell response to canertinib. Biotechnology and Bioengineering. 2012; 109:213–24. [PubMed: 21830205]
38. Falcão-Júnior JOA, Teixeira-Carvalho A, Cândido EB, Lages EL, Ferreira Freitas GG, Lamaita RM, et al. Assessment of chemokine serum levels in epithelial ovarian cancer patients. Tumori. 2013; 99:540–4. [PubMed: 24326845]
39. Burke F, Relf M, Negus R, Balkwill F. A CYTOKINE PROFILE OF NORMAL AND MALIGNANT OVARY. Cytokine. 1996; 8:578–85. [PubMed: 8891439]
40. Negus RP, Stamp GW, Hadley J, Balkwill FR. Quantitative assessment of the leukocyte infiltrate in ovarian cancer and its relationship to the expression of C-C chemokines. The American journal of pathology. 1997; 150:1723–34. [PubMed: 9137096]
41. Hagemann T, Wilson J, Burke F, Kulbe H, Li NF, Pluddemann A, et al. Ovarian cancer cells polarize macrophages toward a tumor-associated phenotype. J Immunol. 2006; 176:5023–32. [PubMed: 16585599]

42. O'Grady NP, Tropea M, Preas HL 2nd, Reda D, Vandivier RW, Banks SM, et al. Detection of macrophage inflammatory protein (MIP)-1alpha and MIP-1beta during experimental endotoxemia and human sepsis. J Infect Dis. 1999; 179:136–41. [PubMed: 9841832]

43. Sousa S, Brion R, Lintunen M, Kronqvist P, Sandholm J, Monkkonen J, et al. Human breast cancer cells educate macrophages toward the M2 activation status. Breast Cancer Res. 2015; 17:101. [PubMed: 26243145]

44. Matte I, Lane D, Bachvarov D, Rancourt C, Piche A. Role of malignant ascites on human mesothelial cells and their gene expression profiles. BMC Cancer. 2014; 14:288. [PubMed: 24761768]

45. Cheaib B, Auguste A, Leary A. The PI3K/Akt/mTOR pathway in ovarian cancer: Therapeutic opportunities and challenges. Chinese Journal of Cancer. 2015; 34:4–16. [PubMed: 25556614]

46. Marshall BT, Long M, Piper JW, Yago T, McEver RP, Zhu C. Direct observation of catch bonds involving cell-adhesion molecules. Nature. 2003; 423:190–3. [PubMed: 12736689]

47. Burgos-Ojeda D, Wu R, McLean K, Chen YC, Talpaz M, Yoon E, et al. CD24+ Ovarian Cancer Cells Are Enriched for Cancer-Initiating Cells and Dependent on JAK2 Signaling for Growth and Metastasis. Mol Cancer Ther. 2015; 14:1717–27. [PubMed: 25969154]

48. Ataga KI, Kutlar A, Kanter J, Liles D, Cancado R, Friedrisch J, et al. Crizanlizumab for the Prevention of Pain Crises in Sickle Cell Disease. N Engl J Med. 2017; 376:429–39. [PubMed: 27959701]

49. Stahli BE, Gebhard C, Duchatelle V, Cournoyer D, Petroni T, Tanguay JF, et al. Effects of the P-Selectin Antagonist Inclacumab on Myocardial Damage After Percutaneous Coronary Intervention According to Timing of Infusion: Insights From the SELECT-ACS Trial. J Am Heart Assoc. 2016; 5

50. Rollins, S., Alvarez, R., Rother, RP., McEver, RP., Kawar, ZS. Anti-P-selectin antibodies. US: 2015. Selexys pharmaceuticals, Oklahoma Medical Research Foundation, assignee.

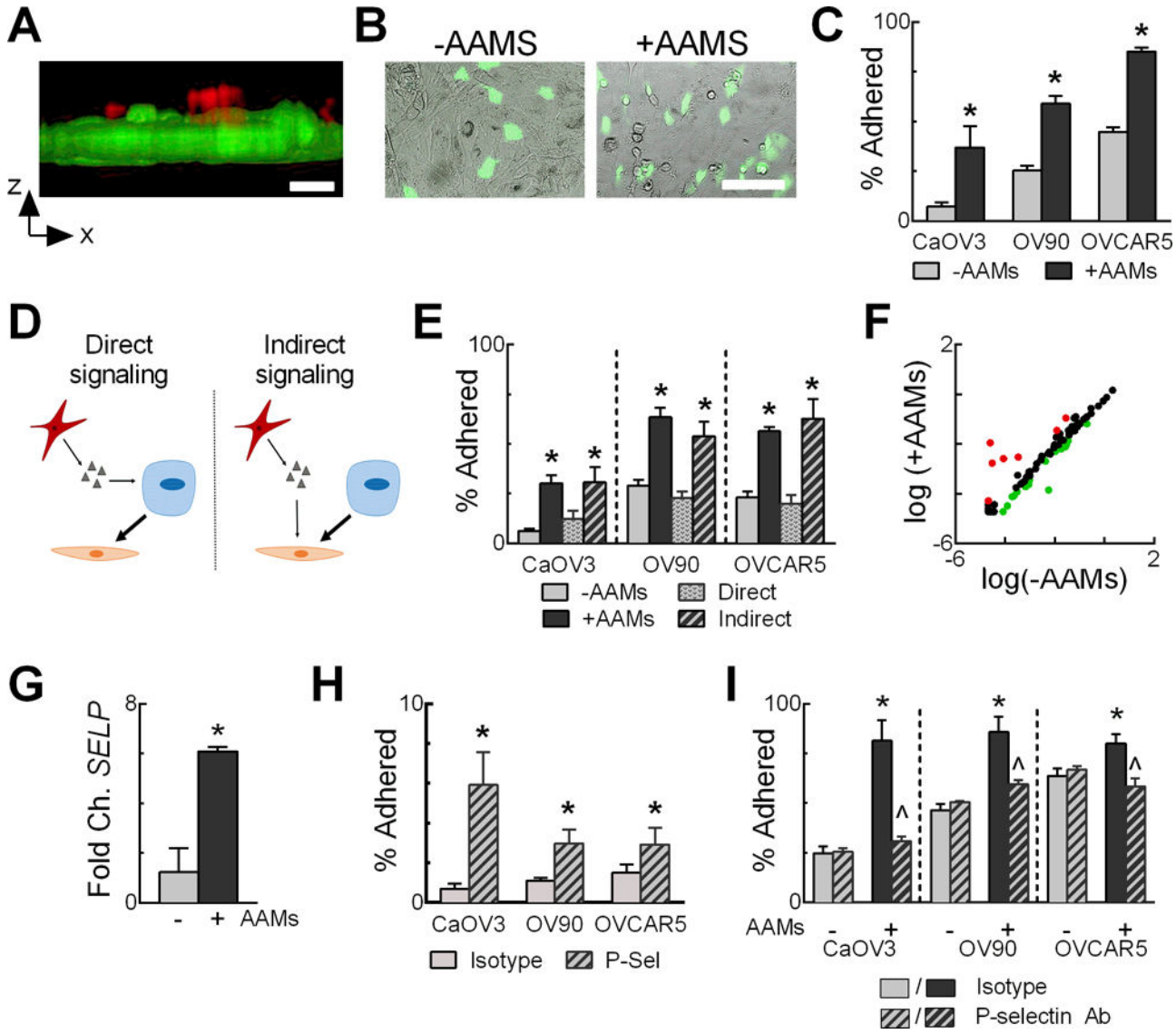

Figure 1. AAMs increase HGSOC adhesion to LP-9 through upregulation of mesothelial P-selectin

(A) Confocal reconstruction of CaOV3 (red) adhered to LP-9 (green). Scale bar=20 μm. (B,C) Representative image (B) of OVCAR5 (green) adhered to LP-9 and quantification (C). Scale bar=100 μm, n=3 replicates, one AAM donor. (D) Potential direct/indirect effects of AAMs. (E) AAMs were included during three-hour adhesion (direct) or during 24-hour time prior to tumor cell addition (indirect), n=3 replicates, one AAM donor. (F) Screen of 86 ECM/adhesion genes from LP-9 cultured in the absence or presence of AAMs for 24 hours. (G) Validation of increased *SELP* in LP-9, n=3 unique AAM donors. (H) Adhesion of HGSOC to adsorbed isotype or P-selectin Fc chimera, n=4. (I) LP-9 in the absence or presence of AAMs were treated with isotype or P-selectin blocking antibody prior to addition of HGSOC. Data is average ± SD, *p<0.05 vs. -AAMs (C,E,G), isotype (H), or –AAMs/isotype (I), ^p<0.05 vs. +AAMs/isotype (I) by two-sided t-test (C,G,H) or two-sided t-test with Bonferroni correction (E,I).

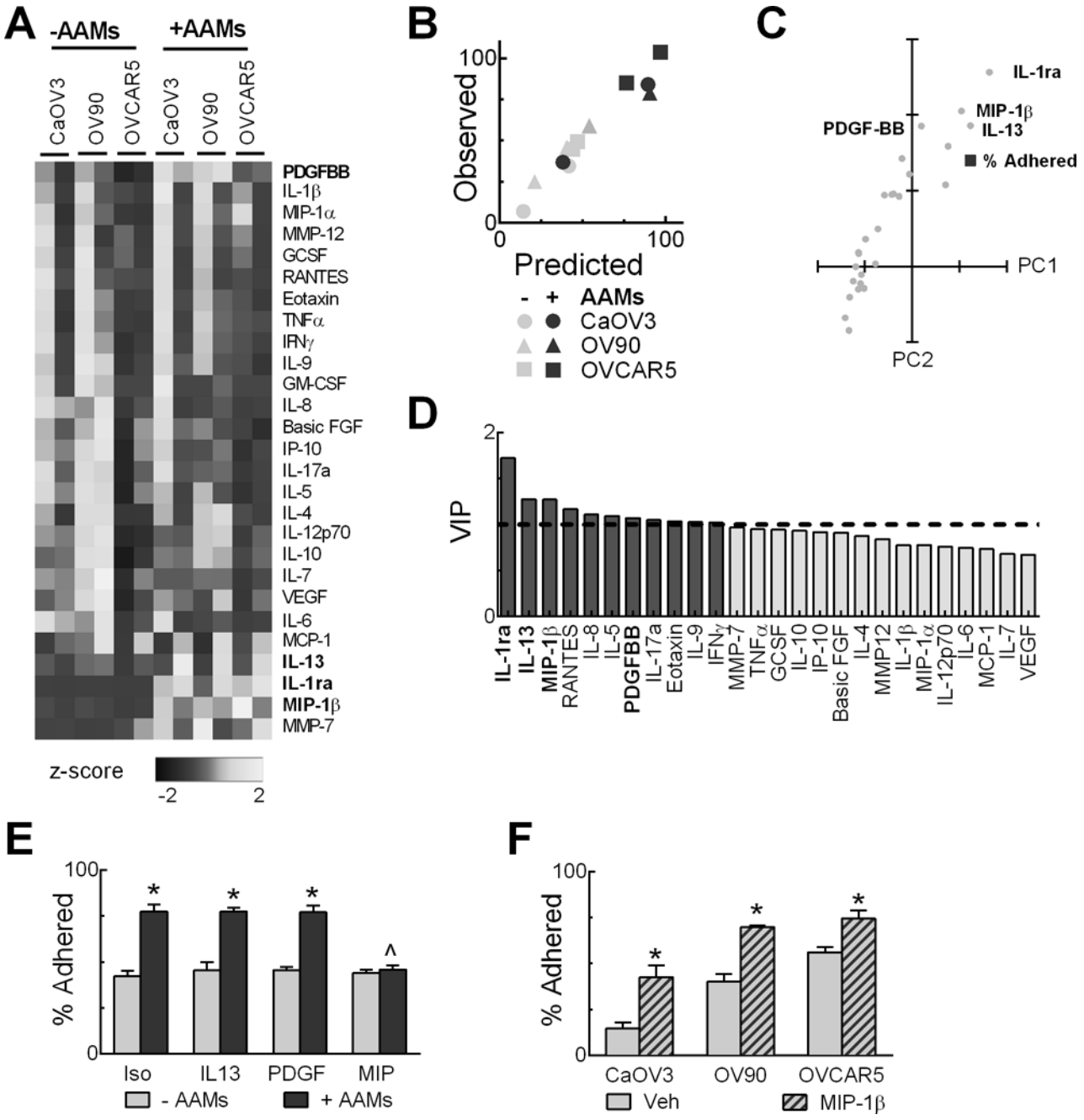

Figure 2. PLSR prediction and experimental validation of role for MIP-1β in increased HGSOC adhesion

(A) Ligands (z-score normalized) detected in the absence or presence of AAMs. Data is average of n=3 replicates per donor, each column represents a unique donor/cell line combination. (B) Comparison of PLSR-predicted to experimentally-observed HGSOC adhesion to LP-9. (C) Correlations of ligands and observed adhesion (% Adhered) with PC1 and PC2 from the PLSR model. (D) VIP>1 (dark grey) indicate important variables to predict adhesion. Those that positively correlated with HGSOC adhesion are shown in bold (and bolded in the heatmap (A) and labeled in (C)). (E) OV90 co-cultures were treated with

neutralizing antibodies against IL-13 (IL13), PDGF-BB (PDGF), MIP-1β (MIP), or isotype (Iso) during co-culture, n=3 replicates, one AAM donor. (F) HGSOC adhesion to LP-9 treated with vehicle or 100 ng/mL MIP-1β, n=3. Data is average ± SD, *$p<0.05$ vs. –AAMs of same isotype/antibody (E) or vehicle (F), ^$p<0.05$ vs. +AAMs/isotype (E) by two-sided t-test (F), with Bonferroni correction (E).

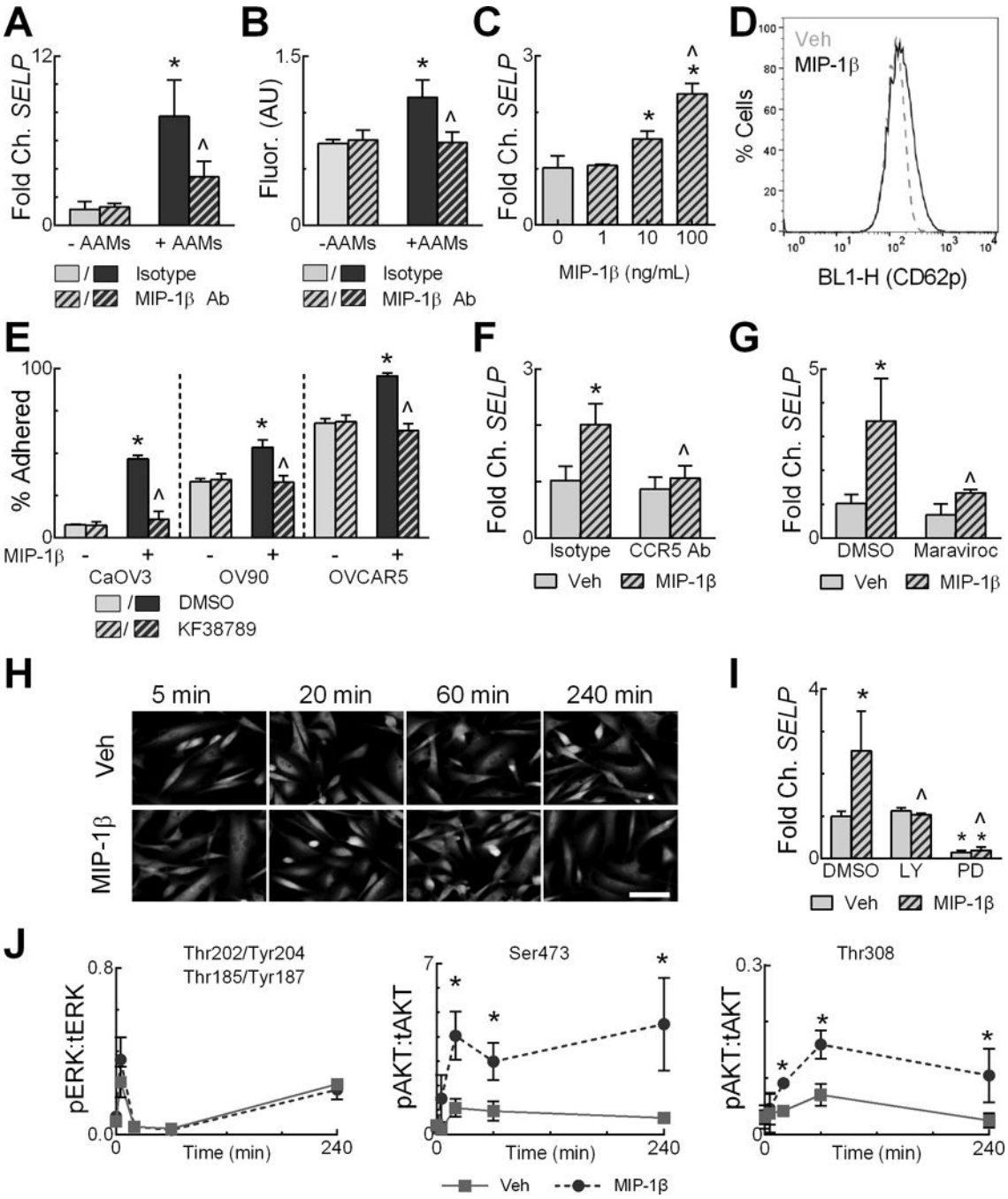

Figure 3. MIP-1β signals through CCR5/PI3K to up-regulate P-selectin

(A,B) Quantification of P-selectin in LP-9 in response to MIP-1β neutralizing antibody or isotype by qRT-PCR (A) and immunofluorescence (B), n=3 replicates, one AAM donor. (C) *SELP* expression in LP-9 after 24 hours of treatment with increasing MIP-1β, n=3. (D) Flow cytometry analysis of P-selectin in LP-9 treated with vehicle or 100 ng/mL MIP-1β (MIP-1β). (E) Treatment of LP-9 with 100 ng/mL MIP-1β and the P-selectin small molecular inhibitor KF38789 demonstrated P-selectin was necessary for MIP-1β increased adhesion, n=3. (F) Treatment of LP-9 with 100 ng/mL MIP-1β and a CCR5 blocking

antibody or isotype demonstrated that CCR5 was necessary for increased *SELP*, n=3. (G) Treatment of LP-9 with 100 ng/mL MIP-1β and maraviroc or DMSO demonstrated that maraviroc negated *SELP* upregulation, n=3. (H) Immunofluorescence of p65 in LP-9 treated with vehicle or 100 ng/mL MIP-1β over time. Scale bar=50 μm. (I) LP-9 were treated with vehicle or 100 ng/mL MIP-1β in combination with DMSO control, 10 μM PI3K (LY) or MEK (PD) inhibitors and *SELP* expression analyzed by qRT-PCR. (J) ERK (Thr202/Tyr204, Thr185/Tyr187) and AKT (Thr308, Ser473) phosphorylation of LP-9 treated with vehicle or 100 ng/mL MIP-1β. Data is average ± SD, *$p<0.05$ vs. –AAMs/isotype (A,B), vehicle (C,J), vehicle/isotype (F), or vehicle/DMSO (E,G,I), ^$p<0.05$ vs. +AAMS/isotype (A,B), 10 ng/mL MIP-1β (C), MIP-1β/isotype (F) or MIP-1β/DMSO (E,G,I) by two-sided t-test with Bonferroni correction (A-C,E-G,I) or two-sided t-test at each time (J).

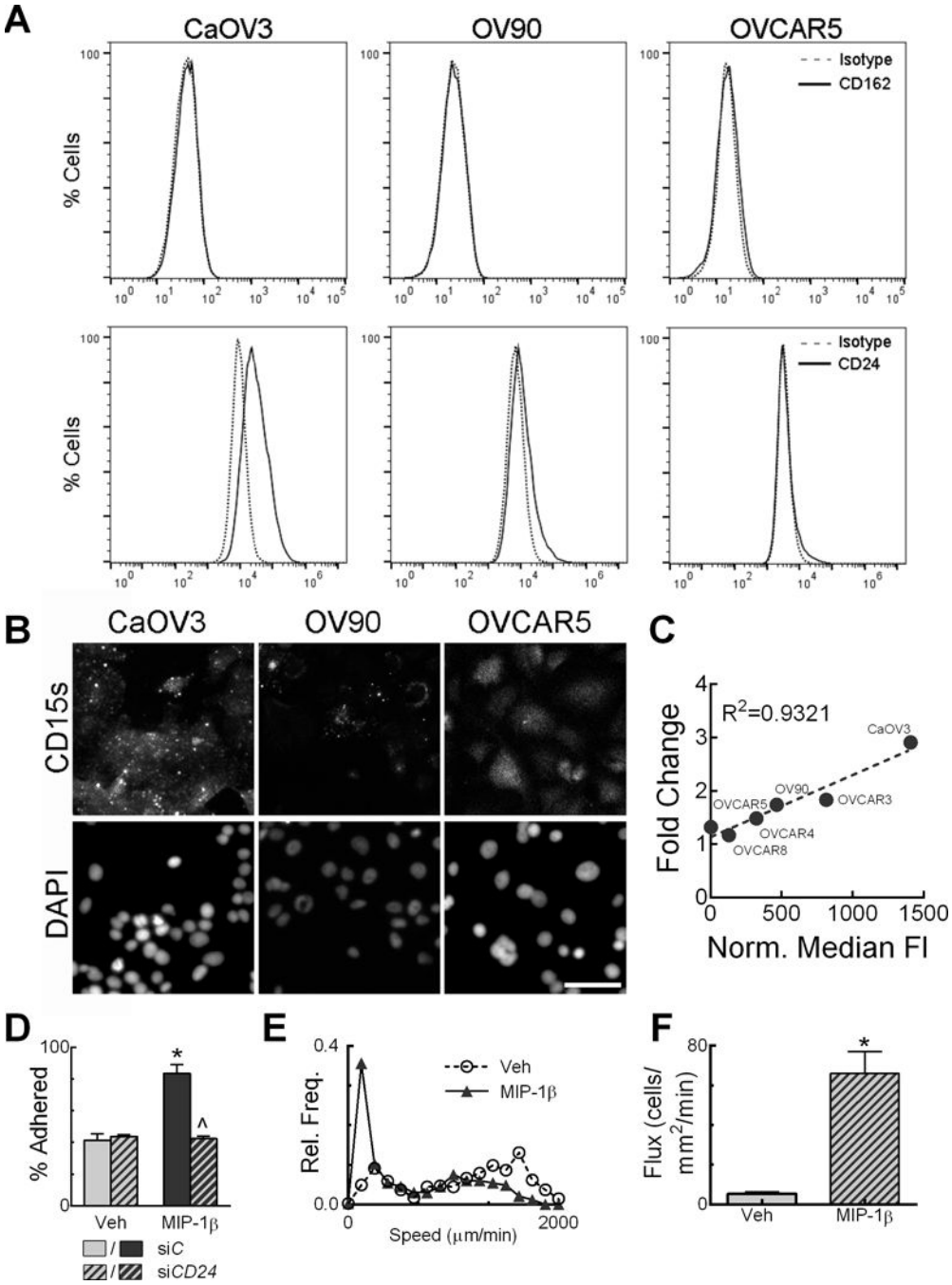

Figure 4. HGSOC cells adhere to P-selectin through CD24

(A) Flow cytometry analysis of CD162 and CD24 in HGSOC cells vs. isotype controls. (B) Representative immunofluorescent staining for CD15s in HGSOC cells. Scale bar=50 μm. (C) Relationship between normalized median CD24 fluorescence from flow cytometry (A, Supplementary Fig. S5A) to fold-change in adhesion to LP-9 treated with MIP-1β. (D) OV90 were treated with si*CD24* or si*C* siRNA and their adhesion to LP-9 treated with vehicle or 100 ng/mL MIP-1β was assayed, n=3. (E) CaOV3 were pumped at 0.125 dyn/cm^2 into parallel flow channels containing LP-9 treated with vehicle or MIP-1β. Cells had a

significantly lower velocity distribution on MIP-1β treated LP-9 compared to vehicle, n=200 cells/condition, $p<0.001$ by Kolmogorov–Smirnov test. (F) Rolling flux of CaOV3 for the conditions in (E), n=200 cells/condition. Data is average ± SD, *$p<0.05$ vs. Veh/si*C* (D) or vehicle (F), ^$p<0.05$ vs. MIP-1β/si*C* (D) by two-sided t-test (F) with Bonferroni correction (D).

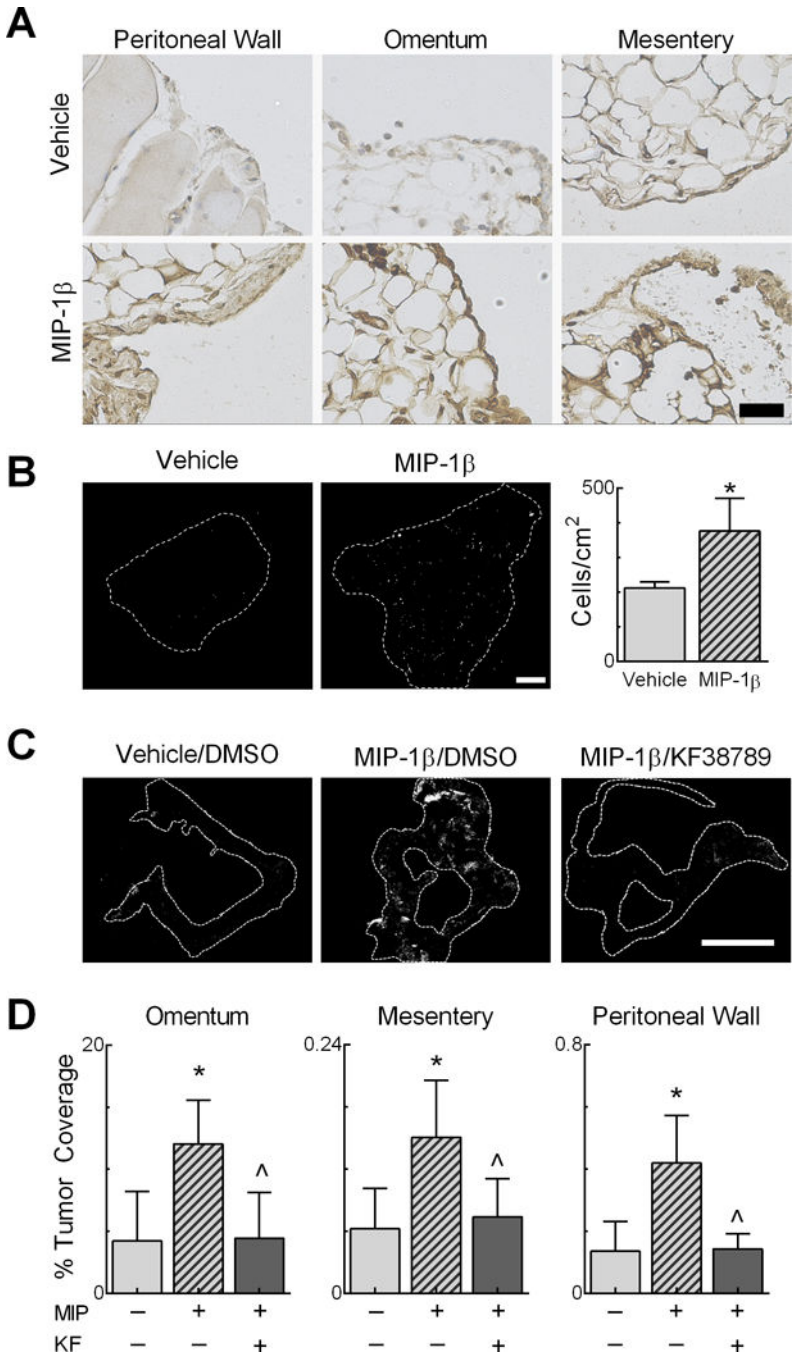

Figure 5. MIP-1β increases P-selectin *in vivo* and adhesion *in vivo* and *ex vivo*

(A) Immunohistochemistry for P-selectin was performed on the peritoneal wall, omentum, and mesentery of mice that were i.p injected with vehicle or 1 μg MIP-1β, scale bar=100 μm. (B) *Ex vivo* adhesion of CaOV3 to peritoneal wall biopsies from mice treated as in (A). Scale bar=1 mm. Images (left) and quantified adhesion (right) from n=3 mice. (D) *In vivo* adhesion of ID8 to the peritoneal wall, omentum, and mesentery was assayed after 90 minutes in mice i.p. injected with vehicle control or 1 μg MIP-1β, followed by DMSO control or KF38789 (1 mg/kg, MIP-1β + KF). Scale bar=0.5 cm. Data is average ± SD, *

p<0.05 vs. vehicle (B), or vehicle/DMSO (D), ^ p<0.05 vs. MIP-1β/DMSO by a two-sided t-test (B) with Bonferroni correction (D).

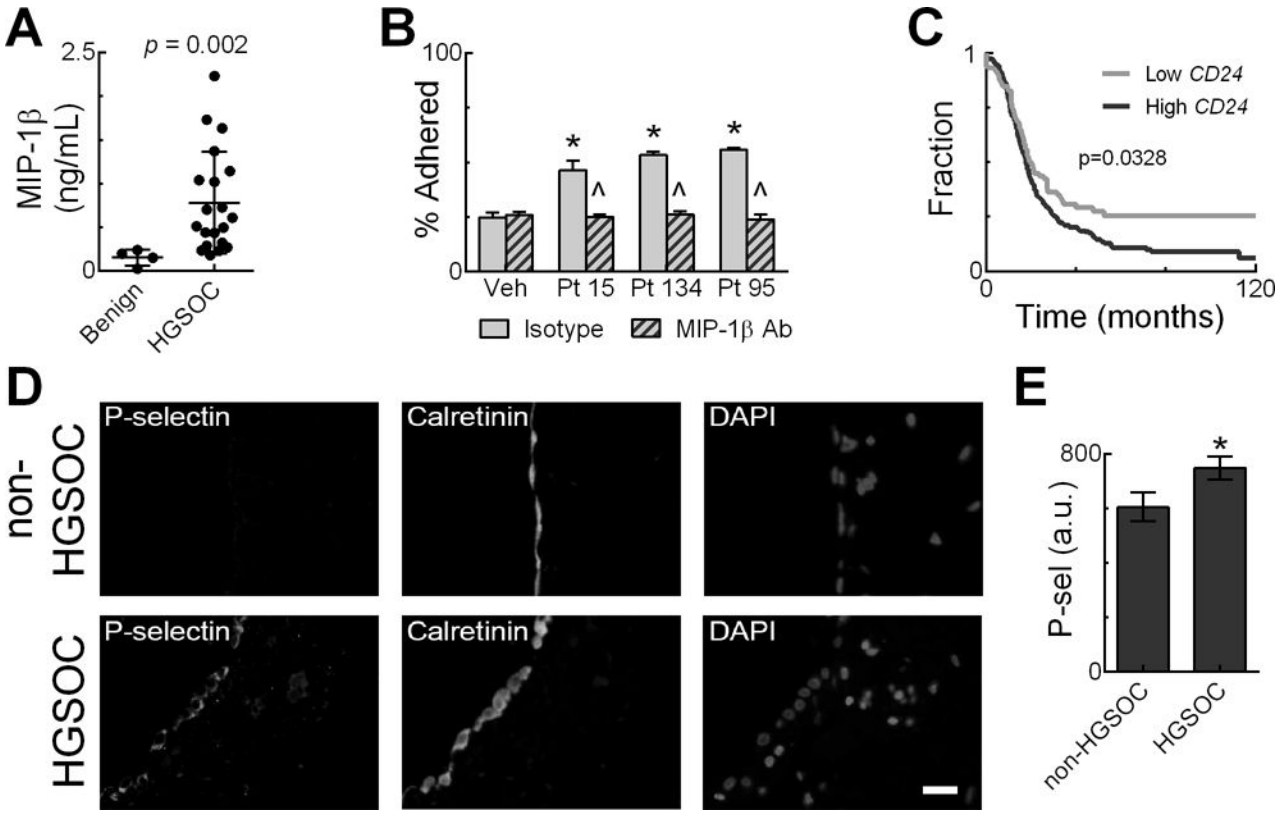

Figure 6. HGSOC patients have elevated MIP-1β and P-selectin

(A) HGSOC ascites had elevated MIP-1β concentrations compared to benign conditions. n=4 benign, n=20 HGSOC. (B) LP-9 were treated with 10% (v/v) of PBS (Veh) or ascites in SFM in conjunction with an isotype control or MIP-1β blocking antibody for 24 hours, n=3 for each patient sample with OV90 cell line. (C) The Kaplan-Meier plotter tool (38) was utilized with Gene Omnibus and The Cancer Genome Atlas databases to calculate PFS for HGSOC patients with low and high expression of *CD24*. (D) Representative omental tissue sections from patients with non-HGSOC or HGSOC conditions stained for P-selectin and calretinin (mesothelial cells). Scale bar=25 μm. (E) Quantification of P-selectin levels in the mesothelium (calretinin-positive) normalized to mesothelium area, n=3 patients/category. Data is average ± SD, * $p<0.05$ vs. non-HGSOC samples (A,E), or vehicle/isotype (B), ^ $p<0.05$ vs. corresponding patient ascites/isotype (B) by two-sided t-test (A,E) with Bonferroni correction (B), or log-rank test (C).